Journal of Medicinal Chemistry

ARTICLE

pubs.acs.org/jmc

Synthesis of New (−)-Bestatin-Based Inhibitor Libraries Reveals a Novel Binding Mode in the S1 Pocket of the Essential Malaria M1 Metalloaminopeptidase†

Geetha Velmourougane,[‡] Michael B. Harbut,[‡] Seema Dalal,[§] Sheena McGowan,[∥] Christine A. Oellig,[∥] Nataline Meinhardt,[‡] James C. Whisstock,[∥] Michael Klemba,[§] and Doron C. Greenbaum*[,‡]

[‡]Department of Pharmacology, University of Pennsylvania, 433 South University Avenue, 304G Lynch Laboratories, Philadelphia, Pennsylvania 19104-6018, United States

[§]Department of Biochemistry, Virginia Polytechnic Institute and State University, 306 Engel Hall, Blacksburg, Virginia 24061, United States

[∥]Department of Biochemistry and Molecular Biology and Australian Research Council Centre of Excellence in Structural and Functional Microbial Genomics, Monash University, Clayton, VIC 3800, Australia

Supporting Information

ABSTRACT: The malarial PfA-M1 metalloaminopeptidase is considered a putative drug target. The natural product dipeptide mimetic, bestatin, is a potent inhibitor of PfA-M1. Herein we present a new, efficient, and high-yielding protocol for the synthesis of bestatin derivatives from natural and unnatural *N*-Boc-D-amino acids. A diverse library of bestatin derivatives was synthesized with variants at the side chain of either the α-hydroxy-β-amino acid (P1) or the adjacent natural α-amino acid (P1′). Surprisingly, we found that extended aromatic side chains at the P1 position resulted in potent inhibition against PfA-M1. To understand these data, we determined the X-ray cocrystal structures of PfA-M1 with two derivatives having either a Tyr(OMe) **15** or Tyr(OBzl) **16** at the P1 position and observed substantial inhibitor-induced rearrangement of the primary loop within the PfA-M1 pocket that interacts with the P1 side chain. Our data provide important insights for the rational design of more potent and selective inhibitors of this enzyme that may eventually lead to new therapies for malaria.

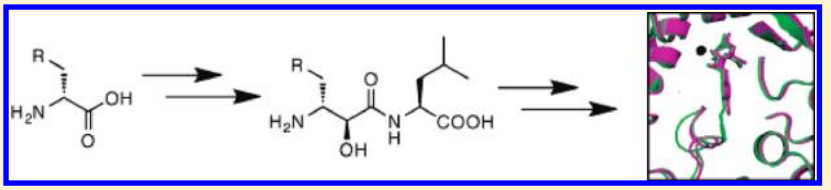

INTRODUCTION

The human parasitic pathogen *Plasmodium falciparum* accounts for most of the 1−2 million malaria related deaths per year.[1] This parasite has a complex life cycle involving several stages of growth, including a mosquito vector stage and a mammalian stage. The human asexual erythrocytic phase (blood stage) is the cause of malaria-associated pathology. The blood stage is a recurring lytic cycle lasting 48 h, wherein vast amounts of host hemoglobin are taken up by the parasite for mostly metabolic purposes.[2] The roles of many endopeptidases, such as the digestive vacuole plasmepsins and falcipains, have been well established, however, these endopeptidases appear to be largely redundant.[3] Interest has recently increased in understanding the roles of aminopeptidases, several of which are genetically essential and may contribute to several biological processes, including the breakdown of hemoglobin and the removal of the terminal methionine from newly synthesized proteins.

Among the 100 peptidases in the *P. falciparum* genome, there are eight metallo-aminopeptidases (MAPs). Four of these are methionine aminopeptidases that presumably have a housekeeping role in the removal of the initiator methionine from newly synthesized polypeptides.[4,5] Of the remaining four peptidases, PfA-M1 (aminopeptidase N; M1 family) is thought to be an essential parasite enzyme and a potential therapeutic target.[6] The *P. falciparum* PfA-M1 enzyme shares low percentage identity (26%) to its human orthologue, aminopeptidase N, highlighting that targeting this essential parasite peptidase over human enzymes may be possible. It is noteworthy that there are some conserved amino acids around the active site, especially those that comprise and surround the HEXXH Zn binding site motif, however, the amino acids comprising the binding pockets show significant diversity.

MAPs catalyze cleavage on the amino terminal of peptide chains. These enzymes are widely distributed in organisms from bacteria to human and play essential roles in protein maturation and regulation of the metabolism of bioactive peptides.[7−9] Although the MAP superfamily is quite large and divergent, most enzymes share a common mechanism, exploiting the coordination of one or two Zn atoms in the active site to activate water for nucleophilic attack of a peptide or protein substrate. Inhibitors of this superfamily therefore tend to incorporate a Zn-binding group into a peptide-like structure. There have been several inhibitor scaffolds used to target the MAP family including, most prominently, phosphinic acids,[10] hydroxamic

Received: September 21, 2010
Published: March 02, 2011

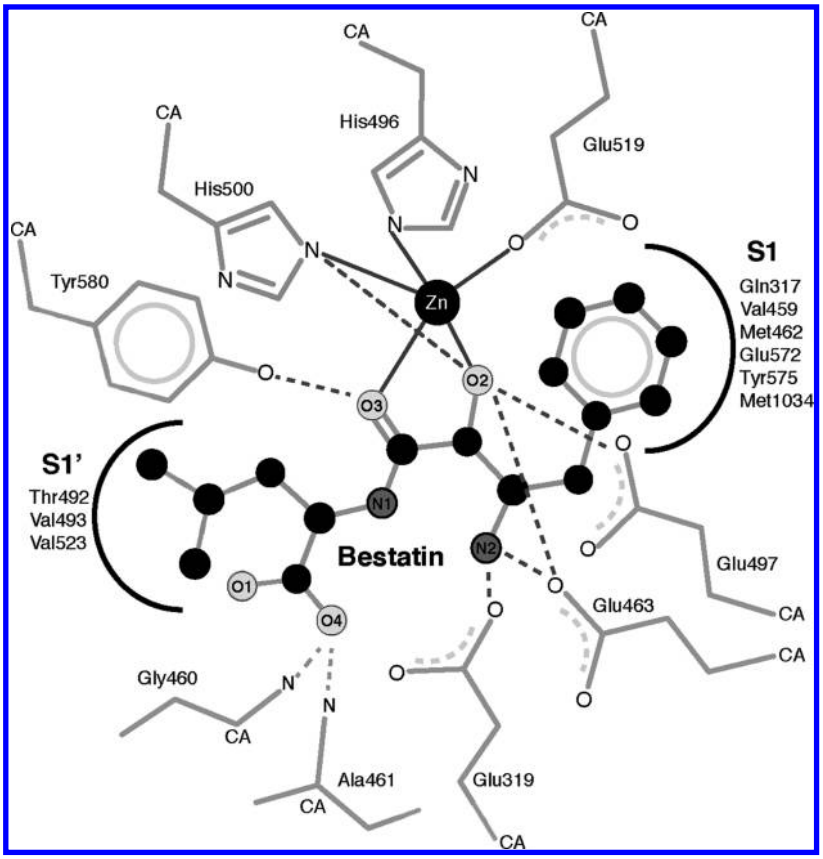

Figure 1. Schematic of bestatin binding to the active site of PfA-M1. S1 and S1′ represent canonical peptidase binding pockets. Residues that comprise the S1 and S1′ pockets are listed alongside the half moon circle. PfA-M1 side chains are represented by numbered amino acids. Solid lines = metallo-bonds; dashed lines = hydrogen bonds; CA = α-carbon. Black spheres represent carbon atoms.

acids,[11] and the bestatin family.[12,13] Both phosphinic acids and hydroxamic acids have the capacity to inhibit metallo-endopeptidases and peptide deformylase and therefore will be intrinsically more difficult to design in specificity for a target MAP. Thus, we focused on the bestatin scaffold because it is synthetically tractable, potent, and specific for the MAP family.

(−)-Bestatin is a natural product of actinomycetes that potently inhibits multiple families of metallo-aminopeptidases (MAPs), including the M1, M17, and M18 families.[14−17] Bestatin has been shown to modulate many biological pathways; importantly, bestatin has been shown to inhibit growth of *P. falciparum* parasites in culture.[18] However, bestatin type inhibitors have not been exploited widely for construction of inhibitor libraries and have not been developed for use as activity-based probes. Moreover, few if any specific inhibitors have been designed for MAPs from any organism regardless of scaffold.[19] We therefore aimed to diversify the main binding determinants of bestatin in order to expand the repertoire of tools with which to study MAPs. We specifically aimed to explore structure−activity relationships with PfA-M1 as a first step toward optimizing the potency of bestatin-like inhibitors against this enzyme.

Bestatin resembles a Phe-Leu dipeptide substrate; however, the first residue contains a α-hydroxy-β-amino acid. Bestatin-based inhibitors coordinate the active zinc atom of MAPs and also form interactions using the side chains of both the α-hydroxy-β-amino acid and the adjacent alpha amino acid which bind into the S1 and S1′ active site pockets of the target enzyme, respectively. Furthermore, the amide between the two amino acids of bestatin forms hydrogen bonds with the enzyme backbone and in some cases one or more MAP glutamate residues coordinate the free amine of bestatin, as highlighted in a recent structure for *Escherichia coli* aminopeptidase N.[17] A recent cocrystal structure of bestatin bound to malaria PfA-M1 enzyme revealed a similar set of interactions between the enzyme and the inhibitor (Figure 1).[20] Bestatin interacts with MAPs in a noncovalent, reversible manner, and in some cases is a slow-binding inhibitor, with initial formation of a low-affinity complex followed by a slow conformational change leading to a high affinity complex.[12,13]

We previously developed a solid-phase strategy that allows for the diversification of the P1′ position of bestatin.[21] Herein we seek to expand on this previous work by the development of a facile and general method for the preparation of bestatin analogues that are diversified both at the leucine (P1′) and at the α-hydroxy-β-amino acid position (P1). We develop a small, directed inhibitor library to explore potency determinants at the S1 and the S1′ pocket against the essential malaria M1-family aminopeptidase, PfA-M1, via kinetic and structural analysis and live parasite assays.

RESULTS

Chemistry. Stemming from the previous work, we wanted to design a simple solid-phase strategy for the synthesis of (−)-bestatin and its P1/P1′ derivatives for library generation (Schemes 1,3). We decided to utilize a Boc protection strategy at the amino group for cleavage from Wang resin, which allows the generation of the final product in one pot.

Construction of P1′ Bestatin Library. Our initial aim was to construct a diverse set of compounds by changing the amino acid

Scheme 1. Synthesis of Bestatin P1′ Derivatives

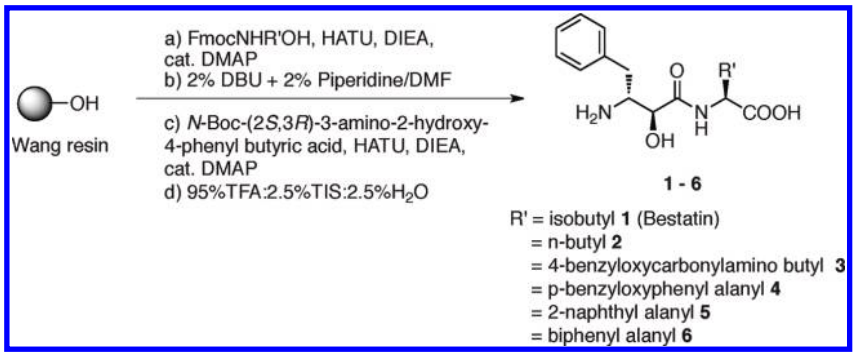

at the P1′ position of bestatin. Accordingly, a library of P1′ bestatin derivatives were synthesized employing solid-phase peptide synthesis as depicted in Scheme 1. We chose to use Wang resin to obtain the product with a C-terminal carboxylate. Norleucine, lysine(Z), *p*-benzyloxy phenyl alanyl, 2-naphthyl alanyl, and biphenyl alanyl amino acids were coupled to the Wang resin using HATU, DIEA, and catalytic DMAP. Fmoc cleavage was achieved using 2%DBU + 2%DIEA in DMF for 20 min. Coupling of the α-hydroxy-*β*-amino acid required HATU in DIEA for 1 h. Cleavage of the resin using 95%TFA:2.5%TIS:2.5%H_2O yielded the bestatin analogues **1**−**6** in 60−70% yields.

Synthetic Strategy for α-Hydroxy-β-amino Acids for P1 Bestatin Library. After successful completion of the P1′ library, we were interested in exploring specificity determinants at the P1 amino acid side chain, which requires the synthesis of α-hydroxy-*β*-amino acids. There have been several noteworthy routes reported for the synthesis of α-hydroxy-*β*-amino acids, all with limitations, including incompatibility with Boc solid-phase chemistry, which led us to develop a more practical approach. Previous routes include: (i) chiron approaches starting from amino acids[22−25] or sugars,[26−29] (ii) asymmetric catalysis,[30,31] (iii) amino hydroxylation,[32,33] (iv) selective reduction of ketones,[34] and (v) chemoenzymolysis.[35,36] The Passerini approach[37] (a one-pot, three-component reaction) for the synthesis of (−)-Bestatin gave a 1.5:1 mixture of diastereomers at the hydroxy center but is limited by difficulties in producing isocyanides in high yields and is severely limited in side chain options. Homologation of α-amino aldehydes via cyanohydrin is not feasible with a Boc protection at the amine.[38] Last, a majority of the methods reported utilized expensive chiral catalysts, had lengthy preparations due to many reaction steps, were low yielding, and were not feasible with a Boc protection on the amino group. Herein we report a simple, efficient, and high yielding approach for the synthesis of the α-hydroxy-*β*-amino acid for bestatin and its P1 derivatives (Scheme 2).

The key intermediate α-hydroxy-*β*-amino acid **13a**−**h** was prepared in five steps from commercially available D-amino acid **7**. The transformation began with the conversion of *N*-Boc-D-amino acids **7a**−**h** into Weinreb amides **8a**−**h** using *N*-methyl morpholine, EDAC·HCl, and *N*,*O*-dimethyl hydroxyl amine hydrochloride in dichloromethane.[39] The use of a Weinreb amide is advantageous in that it readily gives an aldehyde upon treatment with a reducing agent without loss of optical purity. Reduction of the Weinreb amide **8a**−**h** using lithium aluminum hydride in ether at −33 °C yielded the aldehyde **9a**−**h**.[40] Wittig methylenation of α-amino aldehydes using *n*-butyllithium and methyltriphenyl phosphonium bromide in tetrahydrofuran gave a complex mixture of products. We employed the olefination reaction under salt-free Wittig conditions using potassium bis(trimethylsilyl)amide (KHMDS) as a base to give the olefin **10a**−**h**.[41] Dihydroxylation of the alkene **10a**−**h** with osmium tetroxide and *N*-methylmorpholine *N*-oxide gave a diastereomeric mixture of the diol **11a**−**h**.[42] We explored the usage of AD-mix-α and methane sulfonamide in *t*-BuOH:H_2O (1:1) for dihydroxylation reaction, but it did not significantly enhance the selectivity. The diastereomeric ratios of the diols obtained (2*S*,3*R* and 2*R*,3*R*) when AD-mix-α was used as the dihydroxylating agent is reported in Supporting Information Table 1. The crude diol **11a**−**h** was selectively oxidized at the primary hydroxyl functionality to the α-hydroxy-*β*-amino acid **12**:**13** using TEMPO, $NaClO_2$, and NaOCl in NaH_2PO_4.[43,44] Surprisingly, the secondary alcohol remained intact under the oxidation conditions (Scheme 2). Given prior published data that the (2*S*,3*R*) diastereomers of bestatin are much more inhibitory than the corresponding (2*R*,3*R*) diastereomer,[45,46] the active (2*S*,3*R*) diastereomers **13a**−**h** were purified by reverse phase HPLC. The ^{1}H NMR spectra of the **13a**−**h** (2*S*,3*R*) diastereomers had the −NH (doublet) and −Boc (singlet) protons shift at similar ppm in all the examples under study in comparison to the phenyl derivative which is well studied (except for the diphenyl and *n*-propyl, where one diastereomer was exclusively formed). A detailed study showing the shift of −NH and −Boc protons of the α-hydroxy-*β*-amino acids (individual diastereomers) is listed in Supporting Information Table 1. This synthesis is a straightforward method for the preparation of α-hydroxy-*β*-amino acids from α-D-amino acids with good yields.

Construction of P1 Bestatin Library. The α-hydroxy-*β*-amino acids **13a**−**h** were converted to bestatin P1 derivatives via coupling with preloaded Fmoc-Leu Wang resin using HATU and DIEA. Cleavage of the Fmoc group was achieved using 20% piperidine in DMF. Global deprotection of the Boc group and cleavage from Wang resin was accomplished using 95% TFA:2.5%TIS:2.5%H_2O, which gave bestatin **1** and its P1 derivatives **14**−**20** in good yields ranging from 60% to 70% (Scheme 3). Prior work demonstrated that the *Pf*A-M1 MAP had broad specificity,[47] however, published structural data with bestatin demonstrated that the S1 pocket was lined with hydrophobic residues packing well around the P1 Phe side chain (Figure.1).[46] Using this information, we synthesized bestatin derivatives using a series of α-hydroxy-*β*-amino acids consisting of aliphatic and aromatic side chains in increasing size and rigidity. To make use of these new α-hydroxy-*β*-amino acids, we synthesized a library on preloaded Wang resin wherein the second position (P1′) was fixed to a leucine, the amino acid yielding the most potent activity against PfA-M1 at this position. Ultimately, we developed a small library to probe the structure−activity relationships of this P1

dx.doi.org/10.1021/jm101227t |*J. Med. Chem.* 2011, 54, 1655–1666

Scheme 2. Synthesis of α Hydroxy β Amino Acids

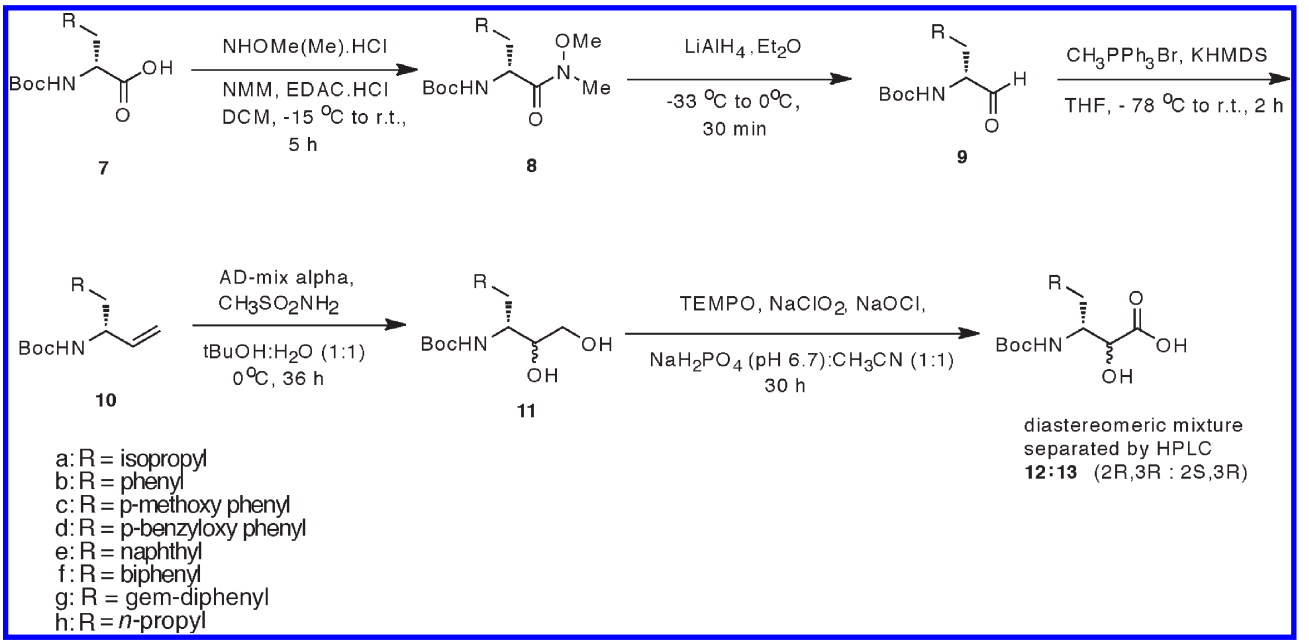

Scheme 3. Synthesis of Bestatin and Its P1 Derivatives

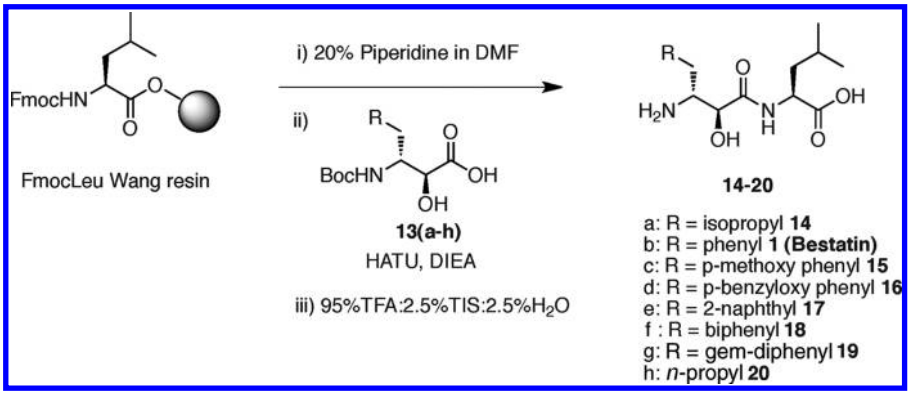

bestatin side chain with the S1 binding pocket of the target enzyme PfA-M1.

Biological Results. *P1′ and P1 Bestatin Library Screening.* To explore interactions between the side chains at the P1 and P1′ sites on the bestatin scaffold with the enzyme, a series of focused inhibitor libraries were synthesized using natural and non-natural aliphatic and aromatic side chains of differing length and rigidity (Schemes 1−3). The P1′ library was first tested in vitro against recombinant PfA-M1 and showed a trend that favored small hydrophobic residues at this site, with leucine displaying the most potent activity (Table 1).

The P1 bestatin library was constructed with a P′ leucine, which yielded the most potent activity against PfA-M1. All inhibitors were again tested in vitro against recombinant PfA-M1. From this data, it was observed that aliphatics, such as a leucine or norleucine, yielded poor inhibitors against the enzyme unlike peptide substrates (Table 2).[47] Interestingly, some larger aromatic substitutions at P1, such as Tyr(OBzl) (**16**) or Tyr(OMe) (**15**), were found to be potent. In fact, **15** was observed to be 5-fold more potent than the parental bestatin with a K_i of 43 nM. Larger rigid aromatic structures, such as naphthyl or biphenyl substituents, rendered inhibitors inactive, which may indicate that the lack of flexibility of these side chains caused an unavoidable steric clash with the target enzyme. However, more flexible large aromatic side chains, such as Tyr(OBzl) (**16**), were quite potent against the enzyme, which is unexpected given that the structure of PfA-M1 and homologous enzymes suggested that the S1 pocket would be unlikely to accommodate side chains much larger than phenylalanine.[20] Last, basic substituents such as lysine were also inactive (not shown), which is surprising given that P1 lysine-containing peptide substrates are processed by PfA-M1 because there is a glutamate at the top of the S1 pocket.[20] However, discrepancies between peptide substrates and bestatin analogues are not surprising, as bestatin contains a α-hydroxy-β-amino acid and thus presents the P1 side chain in a different manner than do peptide substrates.[17]

All P1 inhibitors were then tested against live cultures of *P. falciparum*. The most potent inhibitors found in the in vitro studies also showed moderate potency against *P. falciparum* in culture with IC_{50} values in the micromolar range (Table 2). The most potent compound Tyr(OMe) (**15**) against the enzyme was found to have an IC_{50} around 6 μM against parasites, which was

dx.doi.org/10.1021/jm101227t |J. Med. Chem. 2011, 54, 1655–1666

Table 1. Potency of Bestatin P1′ Derivatives against Recombinant PfA-M1[a]

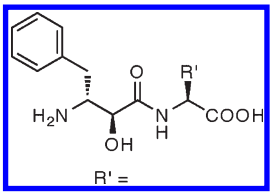

		K_i (nM) PfA-M1
isobutyl (bestatin)	**1**	190
n-butyl	**2**	900
4-benzyloxycarbonyl amino butyl	**3**	1450
p-benzyloxyphenyl alanyl	**4**	>15000
2-naphthyl alanyl	**5**	>15000
biphenyl alanyl	**6**	>15000

[a] Each K_i value as determined from assays at 8 inhibitor concentrations spanning the range 0.014−30 μM (except bestatin; see legend to Table 2).

slightly less potent than bestatin, perhaps due to the lowered permeability caused by the increased hydrophilicity with the introduction of the methoxy group. In addition, another *Plasmodium* aminopeptidase, Pf-LAP, is known to be targeted by bestatin, which could account for the difference between IC_{50} values and in vitro data.

*Structural Analysis of Bestatin Derivatives **15** and **16** Bound to PfA-M1.* The X-ray crystal structure of PfA-M1 bound to bestatin revealed that the S1 subsite in the enzyme accommodated a P1 phenylalanine well with tight packing of enzyme side chains around the phenylalanine side chain.[20] The S1 pocket is lined by hydrophobic residues (Val459, Tyr575, Met1034) and a single polar residue (Glu572). Residues 570−575 (including Glu572 and Tyr575) are located on a loop central to the active site of the enzyme. Comparison of the unbound versus the bestatin-bound PfA-M1 complex revealed that the side chain of only one of the residues (Met1034) that lines the PfA-M1 S1 pocket, moved slightly upon ligand binding. It was thus somewhat surprising that substitution of the bestatin P1 Phe position with larger groups, Tyr(OMe) **15** or Tyr(OBzl) **16**, which we would predict would sterically clash with the enzyme, resulted in molecules with good inhibitory activity.

To address this question, we determined the 1.8 Å X-ray crystal structures of PfA-M1 bound to compounds **15** and **16** (Figure 2). Comparison of these cocrystal structures with that of bestatin-bound PfA-M1 revealed that the S1 pocket of the enzyme is capable of undergoing a major conformational change in response to binding a larger P1 moiety (Figure 2A). Remarkably, when the PfA-M1 enzyme was inhibited by Tyr(OBzl) **16**, the Cα atom of Glu572 moved by ∼5 Å, respectively. In fact, this loop switched to an entirely different conformation with the Cα atom of the neighboring residue, Phe574, moving by ∼1.6 Å. With the smaller **15** compound (Tyr(OMe), this loop movement was less pronounced with the Cα atom of Glu572 moving only 1.2 Å to accommodate the inhibitor. Of note, however, in the latter structure, no electron density was observed for the side chain of Glu572, suggesting a highly mobile side chain. Two of the surrounding residues of the loop (Met571 and Asn573) retain the same conformation as the bestatin-bound enzyme, however, Phe574 also shifts ∼1 Å. In contrast, the S1′ pocket and at the Zn^{2+} atom the interactions are unchanged from that seen

Table 2. Potency of Bestatin P1 Derivatives against Recombinant PfA-M1 and *P. falciparum*[a]

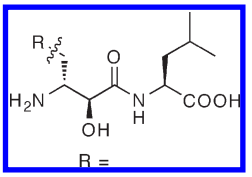

		K_i (nM) PfA-M1	IC_{50} (μM) live parasites
p-methoxy phenyl	**15**	43	6.4
phenyl (bestatin)	**1**	190	3.2
p-benzyloxy phenyl	**16**	490	29
2-naphthyl	**17**	3000	>50
n-propyl	**20**	5300	>50
isopropyl	**14**	NI	>50
biphenyl	**18**	NI	>50
gem-diphenyl	**19**	NI	>50

[a] Each K_i value was determined from assays conducted at four substrate concentrations, each with six concentrations of inhibitor. Duplicate determinations were carried out for compounds **1**, **15**, and **16** and in all cases the replicates were within 12% of the mean. NI = no inhibition

in the bestatin bound structure, with the α-hydroxy group and neighboring carbonyl coordinating the catalytic Zn^{2+}. Accessible surface area calculations revealed that inhibitor **16** also buried a larger surface area (83.7 Å^2) in comparison to **15** (65.5 Å^2) and bestatin (23.8 Å^2, Figure 2B).[20] These accessible surface area maps highlight the significant movement in the S1 pocket of the enzyme to accommodate the larger unnatural side chains.

DISCUSSION

We anticipate that the strategy presented herein for the synthesis of P1 derivatives of bestatin will provide a practical method for a mixed solution and solid-phase route to synthesize novel bestatin-based inhibitors, which will be useful for inhibition of variety of MAPs. During the synthesis, it was surprising that we did not observe better stereoselectivity using the Sharpless AD-mix-α reagent. Because the (2*S*,3*R*) diastereomer was required for good inhibition of PfA-M1, it would be useful to optimize this step in the future. The lack of AD-mix-α stereoselectivity may be due to the steric bulkiness of the R group and the fact that the olefin was terminal.

Screening of the inhibitor libraries revealed that the S1 pocket accommodated some large aromatic side chains well; the (OMe)Tyr derivative (**15**) was the most potent inhibitor, however, the enzyme was able to accommodate a (OBzl)Tyr side chain (**16**), although the K_i decreased, possibly caused by the energetic cost of such a large movement in the enzyme pocket. Given this information, future efforts should be aimed at exploiting the novel binding mode of the P1 α-hydroxy-β-amino acid side chain of bestatin against PfA-M1. Derivatization of the P1 side chain using a wider variety of long hydrophobic side chains between the lengths of compounds **15** and **16** would represent one strategy. In addition, the S1′ pocket favored smaller aliphatic side chains, and thus exploration of a series of small non-natural amino acids at the P1′ position may further increase activity. Other possibilities to enhance the potency against the enzyme and in live cells or animals would entail changing the peptide backbone and, thus, reducing the peptide character of the bestatin pharmacophore.

dx.doi.org/10.1021/jm101227t |*J. Med. Chem.* 2011, 54, 1655–1666

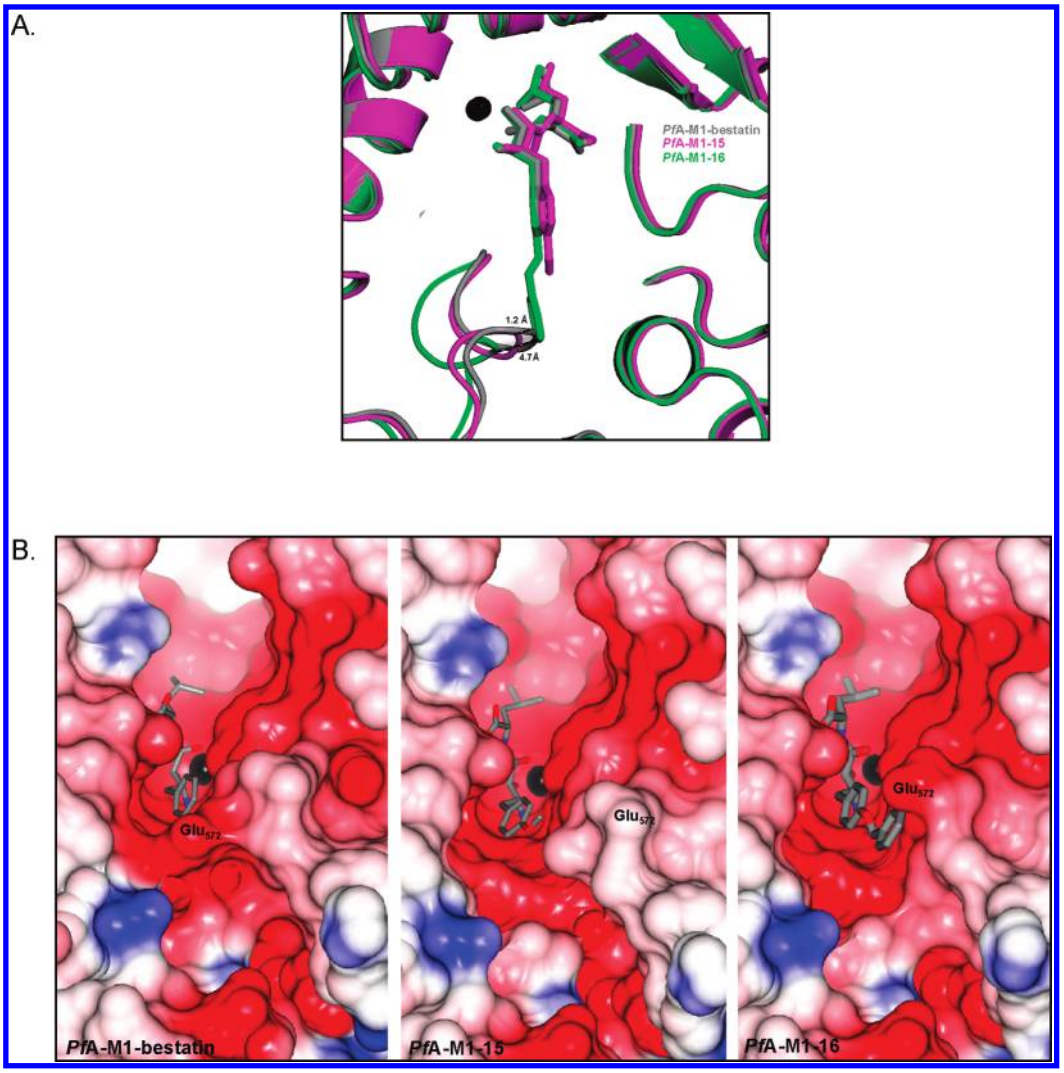

Figure 2. X-ray crystal structures of PfA-M1 bound to Tyr(OMe) (**15**) and Tyr(OBzl) (**16**). (A) Cartoon diagram of the carbon atoms of three X-ray crystal structures of S1 pocket of PfA-M1 bound to bestatin (gray), Tyr(OMe) (**15**) (magenta), and Tyr(OBzl) (**16**) (green). The comparative movement of the Cα-atom of Glu572 is indicated by the dashed lines. (B) The electrostatic potential surface of S1 pocket of PfA-M1 with bestatin, Tyr(OMe) (**15**), and Tyr(OBzl) (**16**) bound in active site. The zinc ion is shown as black sphere, the carbon atoms of inhibitors is in gray, and the position of Glu572 is indicated in each panel. Surfaces were color coded according to electrostatic potential (calculated by the Poisson−Boltzmann solver within CCP4MG). Lys and Arg residues were assigned a single positive charge, and Asp and Glu residues were assigned a single negative charge; all other residues were considered neutral. The calculation was done assuming a uniform dielectric constant of 80 for the solvent and 2 for the protein interior. The ionic strength was set to zero. The color of the surface represents the electrostatic potential at the protein surface, going from blue (potential of $+10\ kT/e$) to red (potential of $-10\ kT/e$), where T is temperature, e is the charge of an electron, and k is the Boltzmann constant. The probe radius used was 1.4 Å.

This can be accomplished in variety of ways, however, the central idea would entail the elimination of the central amide bond between the α-hydroxy-β-amino acid and the leucine to create either: (i) carbapeptides, (ii) azapeptides, or (iii) vinylogous peptides.

Structural analyses of PfA-M1 bound to bestatin, **15** and **16** indicate that the S1 pocket loop is mobile with high B-factors for residues 570−575. Interestingly, structural characterization of PfA-M1 homologues, to date, has not identified this movement in the S1 pocket and do not indicate any enhanced mobility of this region. Taken together, our current SAR data revealed that there is unprecedented plasticity of the S1 binding pocket in the PfA-M1 enzyme that permits the enzyme to accommodate larger side chains and that there is considerably more binding energy to be gained by increasing the size of the original phenylalanyl side chain of the parental bestatin. These data contrast with previous studies on this enzyme family, which generally reveal little change between inhibitor bound and unbound forms.[20] This information is important for future inhibitor design efforts because it may open new routes to building selective inhibitors that target the malaria M1 enzyme over mammalian counterparts.

It is noteworthy that there are 13 M1 family metallo-aminopeptidase members in humans, which may complicate future specificity studies. However, none of the enzymes share much more than ∼26% identity with PfA-M1. Studies on various mammalian M1 orthologues (pig, rat, and human) show significant variation in inhibitor activity between the three closely related enzymes, giving an indication that achieving selectivity is plausible.[48] Aminopeptidase N, the human M1 orthologue most similar to PfA-M1, shares only 26% identity with the *Plasmodium* enzyme with extensive variation at the N- and C-terminal domains, indicating that inhibitor access to the active site may be quite altered. Unfortunately, there is currently no structural information available

for the human M1 enzyme. Ultimately designing inhibitors that are specific for the parasite enzyme over the human M1 family members would be ideal, and there is hope for this possibility considering the low identity between the parasite and human enzymes.

CONCLUSIONS

In conclusion, we believe that this data provides robust data to indicate that the bestatin scaffold provides an excellent pharmacophore for future antimalarial inhibitor development against the PfA-M1 enzyme. Potentially, this scaffold can also be optimized against the other essential MAPs such as the M17 enzyme (Pf-LAP) to generate a single scaffold that potently inhibits multiple enzyme targets, which may reduce the ability of the parasite to generate resistance. Last, evidence that the S1 pocket of this M1 family peptidase is quite flexible upon inhibitor binding may be exploited to develop more potent or selective inhibitors for other members of this family, including other parasitic and human orthologues.

EXPERIMENTAL PROCEDURES

Recombinant PfA-M1. Details of the production of *P. falciparum* PfA-M1 in *E. coli* and its purification will be described elsewhere (D. Ragheb and M. Klemba, manuscript in preparation).

Determination of Inhibitor K_i Values. K_i values for P1′ variants were determined according to the method of Dixon[49] using the fluorogenic substrate L-leucyl-7-amido-4-methylcoumarin (Leu-AMC). Briefly, assays contained 50 mM HEPES pH 7.5, 100 mM NaCl, 0.1% Triton X-100, 0.9 nM PfA-M1, and Leu-AMC concentrations of 12.5, 16.7, 25, and 50 μM in a volume of 200 μL. At each substrate concentration, a range of inhibitor concentrations was assayed, typically ranging from no inhibitor to an inhibitor concentration corresponding to ~4 K_i. Changes in fluorescence were measured in a 96-well plate using a Victor^3 microplate fluorometer (PerkinElmer) equipped with an excitation filter of 380 nm and an emission filter of 460 nm. While bestatin can be a slow-binding inhibitor of some aminopeptidases, we found that a steady state had been attained in the PfA-M1 assays by 40 min. Data were plotted as 1/rate vs inhibitor concentration for each substrate concentration and a linear fit was calculated by nonlinear regression using Kaleidagraph 4.1. A secondary plot was then made with intercepts or slopes vs 1/[S], where S is substrate. The K_i value was determined from the ratio of the slopes of the secondary plots (intercept:slope). Inhibitors were assessed for uncompetitive inhibition by constructing a/v vs i plots.[50] All inhibitors tested exhibited purely competitive inhibition.

K_i values for P1 variants were determined by assaying inhibitors at various concentrations in the range 0.014 to 30 μM with a Leu-AMC concentration of 44 μM. Data were plotted as v_i/v_o vs inhibitor concentration, where v_i is the inhibited rate and v_o is the rate in the absence of inhibitor and fit by nonlinear regression to the expression $v_i/v_o = 1/(1 + [I]/IC_{50})$. K_i was calculated from the formula K_i $IC_{50}/(1 + S/Km)$

Antimalarial Activity Assay. *Plasmodium falciparum* strain 3D7 was cultivated in RPMI 1640 medium (with L-glutamine) containing 20 mM HEPES, 32 mM $NaHCO_3$, and 10% Albumax II (Invitrogen) in erythrocytes at 4% hematocrit.[51] Quantitative assessment of antimalarial activity was determined by measurement of SYBR Green fluorescence. Assays were performed in 96-well black, clear-bottom plates. Briefly, 75 μL of culture (in phenol red-free media RPMI 1640) was aliquoted to each well at a starting parasitemia of 0.5%. Next, serial dilutions of compounds in media were added to each well to bring the final volume to 150 μL. All drugs were assayed in triplicate. Cultures were incubated at 37 °C for 72 h. At the end of incubation 10× lysis buffer (20 mM Tris-HCl, 5 mM EDTA, 0.16% saponin wt/vol, 1.6% Triton X vol/vol) with 10× SYBR Green I (Invitrogen; from 10000 supply) was added to each well and incubated for 1 h at room temperature. Levels of SYBR Green fluorescence, indicating parasite growth, were measured on a Tristar LB 941 microplate reader (Berthold Technologies). IC_{50} values were determined using GraphPad Prism.

X-ray Crystallography. rPfA-M1 enzyme was purified and crystallized as previously described.[20] Crystals of the PfA-M1-15 and PfA-M1-16 complex were obtained by soaking PfA-M1 crystals overnight in mother liquor containing 1 mM ligand. Data were collected at 100 K using synchrotron radiation at the Australian synchrotron microcrystallography beamline 3ID1. Diffraction images were processed using MOSFLM[52] and SCALA[53] from the CCP4 suite.[54] Then 5% of each data set was flagged for calculation of R_{Free}[55] with neither a σ nor a low-resolution cutoff applied to the data. A summary of statistics is provided in Supporting Information Table 2. Subsequent crystallographic and structural analysis was performed using the CCP4i interface[56] to the CCP4 suite,[52] unless stated otherwise. The inhibitor complex was initially solved and refined against the unbound PfA-M1 structure (protein atoms only) as described previously[45] and clearly showed unbiased features in the active site for both structures. Superpositions were performed using MUSTANG.[57] Pymol was used to produce structural representations (http://www.pymol.org).[58] Hydrogen bonds (excluding water-mediated bonds), were calculated using Lig_contact and CONTACT.[54] CCP4MG was used to produce electrostatic diagrams.[48] Stereo diagram of both inhibitors showing electron density is represented in Supporting Information Figure 1. The coordinates and structure factors will be available from the Protein Data Bank (3Q43.pdb and 3Q44.pdb). Raw data and images will be available from TARDIS.[59]

Chemistry. Column chromatography was performed on silica gel, Fisher grade (170−400 mesh). TLC plates were visualized with UV, in an iodine chamber, or with phosphomolybdic acid, ninhydrin unless otherwise noted. Melting points were recorded on a Mel-Temp apparatus and are uncorrected. ^{1}H NMR and ^{13}C NMR spectra were recorded on a Bruker Advance DMX-360 spectrometer. The chemical shifts are reported in parts per million (ppm, δ). The coupling constants are reported in hertz (Hz). The purity of all final compounds was established to be >95% pure by a combination of TLC R_f values in several solvent systems and HPLC. Additionally, the absence of any extraneous peaks in the proton NMR spectrum confirmed the high level of purity. The *N*-Boc-(2*S*,3*R*)-2-hydroxy-3-amino-5-methylhexanoic acid was purchased from CNH technologies.

Solid-phase peptide chemistry was conducted in polypropylene cartridges, with 2-way Nylon stopcocks (Biotage, VA). The cartridges were connected to a 20 port vacuum manifold (Biotage, VA) that was used to drain excess solvent and reagents from the cartridge. HRMS were measured at the University of California Riverside Mass Spectrometry Service Center. All solvents were reagent grade. Unless otherwise stated, all reagents were purchased from commercial sources and used without additional purification. Reverse phase HPLC was conducted on a C18 column using an Agilent 1200 HPLC.

Purifications were performed at room temperature and compounds were eluted with a concentration gradient 0−70% of acetonitrile (0.1% Formic acid). LC/MS data were acquired using N LC/MSD SL system (Agilent). All compounds were purified to greater than 95% purity as assessed by LC analysis (see Supporting Information for LCMS traces).

*General Procedure for the Synthesis of Bestatin (**1**) and Its P1′ Derivatives (**2**−**6**).* Solid-phase peptide synthesis was performed on Wang resin. The first amino acid was coupled to the Wang resin using HATU, DIEA, and cat. DMAP for 1 h. Coupling of the α-hydroxy-β-amino acid required HATU for 1 h. Fmoc protecting group was deprotected with 20% piperidine/DMF (30 min). To cleave products from resin, a solution of 95% TFA:2.5%TIS:2.5%H_2O was added to the resin. After standing for 2 h, the cleavage mixture was collected and the resin was washed with fresh cleavage solution. The combined fractions were evaporated to dryness, and the product was purified by reverse phase-HPLC. Fractions containing product were pooled and lyophilized. The yields of bestatin (**1**) and its derivatives (**2**−**6**) ranged from 60% to 70%, respectively, after HPLC purification.

HRMS calcd for PheNleOH **2** $C_{16}H_{25}N_2O_4$ 309.1809 ($M^+ + H$), found 309.1801.

HRMS calcd for PheLys(Z)OH **3** $C_{24}H_{32}N_3O_6$ 458.2286 ($M^+ + H$), found 458.2278.

HRMS calcd for PheTyr(Bzl)OH **4** $C_{26}H_{29}N_2O_5$ 449.2071 ($M^+ + H$), found 449.2068.

HRMS calcd for PheNaphOH **5** $C_{23}H_{25}N_2O_4$ 393.1809 ($M^+ + H$), found 393.1816.

HRMS calcd for PheBipOH **6** $C_{25}H_{27}N_2O_4$ 419.1965 ($M^+ + H$), found 419.1959.

Synthesis of α-Hydroxy-*β*-aminoacids. *General Procedure for the Synthesis of N-Methoxy-N-methyl Acetamide (Weinreb Amides).* In an oven-dried, 50 mL, two-neck, round-bottom flask equipped with a magnetic stirring bar and argon balloon was placed *N*-Boc-D-amino acid (1.997 g, 6.33 mmol) in dry CH_2Cl_2 (15 mL) and the solution was cooled to −15 °C. *N,O*-Dimethylhydroxylamine hydrochloride (0.636 g, 6.52 mmol) was added, followed by *N*-methylmorpholine (0.72 mL, 6.55 mmol). After 5 min, 1-(3-methylaminopropyl-3-ethylcarbodiimide hydrochloride (1.238 g, 6.46 mmol) was added in five portions over 30 min. The reaction was warmed to room temperature, and after 5 h, H_2O (2 mL) was added and the solution was extracted with CH_2Cl_2 (3 × 5 mL). The combined organic phases were washed with brine (5 mL), dried (Na_2SO_4), and concentrated. The residue was purified by flash chromatography.

(R)-N-(tert-Butoxycarbonyl)-2-amino-3-phenyl-N-methoxy-methylpropionamide (8b). Prepared according to the general procedure and was purified by flash chromatography (*n*-hexane/EtOAc = 5/1) to give **8b** (96%) as an oily liquid; $[\alpha]_D^{25} = -24.26$ ($c = 0.68$, $CHCl_3$). ^{1}H NMR (360 MHz, $CDCl_3$) δ 1.39 (s, 9H), 2.87−2.90 (m, 1H), 3.02−3.08 (m, 1H), 3.16 (s, 3H), 3.66 (s, 3H), 4.94 (br s, 1H), 5.15 (br s, 1H), 7.16−7.30 (m, 5H). ^{13}C NMR (90 MHz, $CDCl_3$) δ 28.5, 32.2, 32.3, 39.1, 51.8, 61.7, 79.8, 127.0, 128.6, 129.7, 136.9, 155.4.

(R)-N-(tert-Butoxycarbonyl)-2-amino-3-(p-methyloxyphenyl)-N-methoxy-N-methylpropionamide (8c). Prepared according to the general procedure and was purified by flash chromatography (*n*-hexane/EtOAc = 5/1) to give **8c** (97%) as an oily liquid; $[\alpha]_D^{25} = -22.12$ ($c = 1.08$, $CHCl_3$). ^{1}H NMR (360 MHz, $CDCl_3$) δ 1.39 (s, 9H), 2.82−2.86 (m, 1H), 2.97−3.02 (m, 1H), 3.16 (s, 3H), 3.66 (s, 3H), 3.77 (s, 3H), 4.90 (br s, 1H), 5.14 (br s, 1H), 6.81 (d, $J = 8.3$ Hz, 2H), 7.08 (d, $J = 8.3$ Hz, 2H). ^{13}C NMR (90 MHz, $CDCl_3$) δ 28.5, 32.3, 38.2, 51.8, 55.4, 61.7, 79.7, 114.0, 128.8, 130.6, 155.4, 158.7. HRMS calcd for $C_{17}H_{27}N_2O_5$ ($M^+ + H$) = 339.1914, found = 339.1912.

(R)-N-(tert-Butoxycarbonyl)-2-amino-3-(p-benzyloxyphenyl)-N-methoxy-N-methylpropionamide (8d). Prepared according to the general procedure and was purified by flash chromatography (*n*-hexane/EtOAc = 5/1) to give **8d** (85%) as a colorless solid; mp 102 °C; $[\alpha]_D^{25} = -14.54$ ($c = 0.55$, $CHCl_3$). ^{1}H NMR (360 MHz, $CDCl_3$) δ 1.39 (s, 9H), 2.80−2.85 (m, 1H), 2.96−3.01 (m, 1H), 3.15 (s, 3H), 3.64 (s, 3H), 4.89 (br s, 1H), 5.02 (s, 2H), 5.13 (s, 1H), 6.88 (d, 2H, $J = 9.0$ Hz), 7.07 (d, 2H, $J = 9.0$ Hz), 7.25−7.42 (m, 5H). ^{13}C NMR (90 MHz, $CDCl_3$) δ 28.5, 32.3, 38.2, 38.2, 51.8, 61.7, 70.2, 79.8, 115.0, 127.6, 128.1, 128.7, 129.2, 130.7, 137.4, 158.0, 207.1. HRMS calcd for $C_{23}H_{30}N_2O_5$ ($M^+ + H$) = 415.2233, found = 415.2229.

(R)-N-(tert-Butoxycarbonyl)-2-amino-3-(2-naphthyl)-N-methoxy-N-methylpropionamide (8e). Prepared according to the general procedure and was purified by flash chromatography (*n*-hexane/EtOAc = 5/1) to give **8e** (93%) as a colorless solid; mp 103 °C; $[\alpha]_D^{25} = -20.19$ ($c = 1.02$, $CHCl_3$). ^{1}H NMR (360 MHz, $CDCl_3$) δ 1.35 (s, 9H), 3.01−3.25 (m, 5H), 3.65 (s, 3H), 5.04 (br s, 1H), 5.20 (br s, 1H), 7.31 (d, $J = 10.0$ Hz, 1H), 7.39−7.46 (m, 2H), 7.62 (s, 1H), 7.75−7.80 (m, 3H). ^{13}C NMR (90 MHz, $CDCl_3$) δ 28.2, 28.5, 32.3, 39.2, 51.7, 61.8, 79.8, 125.7, 126.2, 127.8, 127.8, 128.1, 128.3, 132.6, 133.7, 134.3, 172.6, 207.1.

(R)-N-(tert-Butoxycarbonyl)-2-amino-3-(p-phenylphenyl)-N-methoxy-N-methylpropionamide (8f). Prepared according to the general procedure and was purified by flash chromatography (*n*-hexane/EtOAc = 5/1) to give **8f** (87%) as a colorless solid; mp 106 °C; $[\alpha]_D^{25} = -11.37$ ($c = 0.73$, $CHCl_3$). ^{1}H NMR (360 MHz, $CDCl_3$) δ 1.39 (s, 9H), 2.92−2.94 (m, 1H), 3.07−3.13 (m, 1H), 3.19 (s, 3H), 3.69 (s, 3H), 4.99 (br s, 1H), 5.19 (br s, 1H), 7.23−7.58 (m, 9H). ^{13}C NMR (90 MHz, $CDCl_3$) δ 28.3, 28.5, 32.3, 32.3, 38.7, 38.9, 51.7, 61.8, 79.8, 118.9, 127.2, 127.3, 127.4, 127.6, 128.9,130.1, 135.9, 139.9, 141.2, 145.6, 155.4, 172.5. HRMS calcd for $C_{22}H_{29}N_2O_4$ ($M^+ + H$) = 385.2127, found = 385.2116.

(R)-N-(tert-Butoxycarbonyl)-2-amino-3,3-diphenyl-N-methoxy-N-methylpropionamide (8g). Prepared according to the general procedure and was purified by flash chromatography (*n*-hexane/EtOAc = 4/1) to give **8g** (88%) as a colorless solid; mpt 83 °C. ^{1}H NMR (360 MHz, $CDCl_3$) δ 1.31 (s, 9H), 2.93 (s, 3H), 3.61 (s, 3H), 4.33 (d, 1H, $J = 10.8$ Hz, −N*H*), 5.01 (d, 1H, $J = 10.1$ Hz, −C*H*$(Ph)_2$), 5.68 (t, 1H, $J = 10.1$ Hz, NHC*H*CO), 7.15−7.36 (m, 10H). ^{13}C NMR (90 MHz, $CDCl_3$) δ 28.4, 28.6, 31.9, 52.0, 54.7, 61.9, 79.8, 79.9, 126.9, 127.0, 128.4, 128.6, 128.8, 129.0, 129.4, 140.4, 140.6, 155.2, 172.6. HRMS calcd for $C_{22}H_{29}N_2O_4$ ($M^+ + H$) = 385.2127, found = 385.2119.

(R)-N-(tert-Butoxycarbonyl)-2-amino-3-propyl-N-methoxy-N-methylpropionamide (8h). Prepared according to the general procedure and was purified by flash chromatography (*n*-hexane/EtOAc = 4/1) to give **8h** (90%) as an oily liquid. ^{1}H NMR (360 MHz, $CDCl_3$) δ 0.89 (t, 3H, $J = 6.8$ Hz), 1.26−1.55 (m, 14H), 1.66−1.72 (m, 1H), 3.21 (s, 3H), 3.77 (s, 3H), 1.09 (brs, 1H), 5.15 (d, 1H, $J = 7.6$ Hz).

General Procedure for the Wittig Reaction. In an oven-dried, 50 mL, single-necked, round-bottom flask equipped with a magnetic stirring bar, rubber septum, and argon balloon was placed Weinreb amides (1.860 g, 5.19 mmol) in anhydrous Et_2O (20 mL). The solution was cooled to −33 °C and $LiAlH_4$ (1 M in THF, 6.2 mL, 6.23 mmol) was added dropwise, and the reaction mixture was warmed to 0 °C. After 45 min, the solution was cooled to −33 °C and 10% aq $KHSO_4$ (10 mL) was added to quench the reaction. After warming to room temperature 1 N HCl (10 mL) was added, and the organic phases were separated, the aqueous phase was extracted with EtOAc (2 × 10 mL), and the combined organic phases were dried ($MgSO_4$) and concentrated to yield the crude aldehyde. In a separate 50 mL, single-necked, round-bottom flask was placed methyltriphenylphosphonium bromide (3.65 g, 10.24 mmol) in THF (20 mL), and KHMDS (0.5 M in toluene, 19.5 mL, 9.76 mmol) was added. The resulting yellow suspension was stirred at room temperature for 2 h, then cooled to −78 °C and the crude aldehyde (1.75 g, 5.85 mmol) in THF (5 mL) was added dropwise. It was warmed to room temperature over 2 h and quenched with MeOH (5 mL). The resulting mixture was poured into a mixture of saturated potassium sodium tartarate and water (1:1, 15 mL), extracted with Et_2O (2 × 50 mL), dried ($MgSO_4$), and concentrated. The residue was purified by flash chromatography to afford the respective alkenes.

(R)-N-(tert-Butoxycarbonyl)-3-amino-4-phenyl-1-butene (10b). Prepared according to the general procedure and was purified by flash chromatography (*n*-hexane/EtOAc = 20/1) to give **10b** (71%) as a colorless solid; mp 62 °C; $[\alpha]_D^{25} = -37.19$ ($c = 0.28$, $CHCl_3$). ^{1}H NMR (360 MHz, $CDCl_3$) δ 1.39 (s, 9H), 2.83 (d, $J = 6.5$ Hz, 1H), 4.40 (br s, 1H), 5.05−5.11 (m, 1H), 5.74−5.83 (m, 1H), 7.16−7.30 (m, 5H).

(R)-N-(tert-Butoxycarbonyl)-3-amino-4-(p-methyloxyphenyl)-1-butene (10c). Prepared according to the general procedure and was purified by flash chromatography (*n*-hexane/EtOAc = 20/1) to give **10c** (67%) as a colorless solid; mp 58 °C ; $[\alpha]_D^{25} = -36.33$. ^{1}H NMR (360 MHz, $CDCl_3$) δ 1.41 (s, 9H), 2.77 (d, $J = 6.5$ Hz, 2H), 3.78 (s, 3H), 4.36 (br s, 1H), 5.06−5.12 (m, 2H), 5.74−5.83 (m, 1H), 6.82 (d, $J = 8.6$ Hz, 2H), 7.09 (d, $J = 8.6$ Hz, 2H). ^{13}C NMR (90 MHz, $CDCl_3$) δ 28.6, 40.8, 40.8, 53.8, 54.0, 55.5, 79.6, 114.0, 114.9, 129.6, 130.7, 138.4, 155.5, 158.5. HRMS calcd for $C_{16}H_{24}NO_3$ ($M^+ + H$) = 278.1751, found = 278.1749.

(R)-N-(tert-Butoxycarbonyl)-3-amino-4-(p-benzyloxyphenyl)-1-butene (10d). Prepared according to the general procedure and was purified by flash chromatography (*n*-hexane/EtOAc = 20/1) to give **10d** (71%) as a colorless solid; mp 87 °C; $[\alpha]_D^{25} = -29.62$ ($c = 0.53$, $CHCl_3$). ^{1}H NMR (360 MHz, $CDCl_3$) δ 1.40 (s, 9H), 2.77 (d, $J = 6.7$ Hz, 2H), 4.40 (br s, 1H),

5.04 (s, 2H), 5.06−5.12 (m, 2H), 5.74−5.83 (m, 1H), 6.90 (d, J = 11.2 Hz, 2H), 7.08 (d, J = 11.2 Hz, 2H), 7.30−7.44 (m, 5H). ^{13}C NMR (90 MHz, $CDCl_3$) δ 28.5, 40.7, 53.8, 70.2, 79.4, 114.8, 114.9, 127.6, 128.0, 128.7, 130.0, 130.7, 137.3, 138.4, 155.4, 157.7. HRMS calcd for $C_{22}H_{27}NO_3$ (M^+ + Na) = 376.1889, found 376.1879.

(R)-N-(tert-Butoxycarbonyl)-3-amino-4-(2-naphtyl)-1-butene (10e). Prepared according to the general procedure and was purified by flash chromatography (*n*-hexane/EtOAc = 20/1) to give **10e** (80%) as a colorless solid; mpt 104 °C; $[\alpha]_D^{25}$ = −42.46 (c = 0.32). ^{1}H NMR (360 MHz, $CDCl_3$) δ 1.38 (s, 9H), 2.97−3.01 (m, 2H), 4.50 (br s, 1H), 5.07−5.14 (m, 2H), 5.79−5.87 (m, 1H), 7.33 (d, J = 9.7 Hz, 1H), 7.40−7.47 (m, 2H), 7.63 (s, 1H), 7.76−7.82 (m, 3H). ^{13}C NMR (90 MHz, $CDCl_3$) δ 28.5, 41.9, 53.5, 115.1, 125.7, 126.2, 127.8, 127.8, 128.1, 128.2, 128.3, 132.5, 133.7, 135.2, 138.3, 155.4, *tert*-butyl carbon not observed. HRMS calcd for $C_{19}H_{23}NO_2$ (M^+ + Na) = 320.1624, found 320.1620.

(R)-N-(tert-Butoxycarbonyl)-3-amino-4-(p-phenylphenyl)-1-butene 10f). Prepared according to the general procedure and was purified by flash chromatography (*n*-hexane/EtOAc = 20/1) to give **10f** (67%) as a colorless solid. ^{1}H NMR (360 MHz, $CDCl_3$) δ 1.40 (s, 9H), 2.88 (d, J = 5.8 Hz, 2H), 4.47 (br s, 2H), 5.09−5.16 (m, 2H), 5.79−5.88 (m, 1H), 7.24−7.59 (m, 9H). ^{13}C NMR (90 MHz, $CDCl_3$) δ 28.6, 41.4, 115.0, 127.2, 127.3, 127.4, 129.0, 130.2, 136.8, 138.3, 139.6, 141.1, 155.4.

(R)-N-(tert-Butoxycarbonyl)-3-amino-5,5-diphenyl-1-pentene (10g). Prepared according to the general procedure and was purified by flash chromatography (*n*-hexane/EtOAc = 20/1) to give **10g** (78%) as a colorless solid; mp 98 °C; $[\alpha]_D^{25}$ = −56.89 (c = 0.58, $CHCl_3$). ^{1}H NMR (360 MHz, $CDCl_3$) δ 1.36 (s, 9H), 3.97 (d, J = 9.4 Hz, 2H), 4.39 (br s, 1H), 4.99 (br s, 1H), 5.03−5.16 (m, 2H), 5.71−5.80 (m, 1H), 7.15−7.30 (m, 10H). ^{13}C NMR (90 MHz, $CDCl_3$) δ 28.5, 55.4, 57.0, 115.5, 126.8, 127.0, 128.7, 128.7, 128.8, 128.9, 137.7, 141.8, 155.5, *tert*-butyl carbon not observed. HRMS calcd for $C_{21}H_{25}NO_2$ (M^+ + Na) = 346.1783, found 346.1784.

(R)-N-(tert-Butoxycarbonyl)-3-amino-4-propyl-1-butene (10h). Prepared according to the general procedure and was purified by flash chromatography (*n*-hexane/EtOAc = 20/1) to give **10h** (65%) as an oily liquid. ^{1}H NMR (360 MHz, $CDCl_3$) δ 0.89 (t, 3H, J = 6.8 Hz), 1.27−1.33 (m, 4H), 1.42−1.51 (s, 11H), 4.07 (brs, 1H), 4.53 (brs, 1H), 5.05−5.16 (m, 2H), 5.70−5.77 (m, 1H).

General Method for the Synthesis of α-Hydroxy-β-amino Acid. In an oven-dried, 50 mL, single-necked, round-bottom flask equipped with a magnetic stirring bar, rubber septum, and argon balloon was placed the alkene (1.20 g, 4.33 mmol) in *t*-BuOH:H_2O (12 mL, 1:1) and methanesulfonamide (0.412 g, 4.33 mmol) was added. The reaction mixture was cooled to 0 °C and AD-mix-α (6.54 g) was added. The resulting mixture was stirred at 0 °C for 36 h and at room temperature for 8 h and then quenched with solid Na_2SO_3 (7.0 g) and extracted with ethyl acetate. The organic extracts were washed with NaOH (1M, 10 mL), water and brine, dried (Mg_2SO_4), and concentrated. The crude diol was used as such for the next step.

The residue was dissolved in phosphate buffer (NaH_2PO_4, pH 6.7, 6 mL) and MeCN (6 mL). To the solution was added 2,2,6,6-tetramethylpiperidin-1-oxyl (TEMPO, 0.169 g, 1.07 mmol) and sodium chlorite (0.697 g, 7.71 mmol). The reaction mixture was warmed to 35 °C, and 4% aqueous sodium hypochlorite (NaOCl) solution (0.008 g, 0.12 mmol) was added. The mixture was stirred at this temperature for 6.5 h, and TEMPO (0.053 g, 0.34 mmol) along with 4% aqueous NaOCl solution (0.001 g, 0.02 mmol) were added. After stirring at 35 °C for 24 h, H_2O (5 mL) was added, and the pH of the mixture was adjusted to 8.0 with 2.0 M aqueous NaOH solution. The reaction flask was cooled to 20 °C and 6% aq sodium sulfite was added until the solution had a pH of 9. After warming to rt for 30 min, Et_2O (5 mL) was added and the organic phase was separated. To the aqueous layer 1N HCl was added until the pH of the solution was 3, and extracted with ethyl acetate, washed with brine dried and concentrated to yield the α-hydroxy-β-amino acids. The combined yields of the α-hydroxy-β-amino acids ranged from 65% to 70%. HPLC purification of the mixture provided the individual diastereomers.

(2R,3R)-N-(tert-Butoxycarbonyl)-3-amino-2-hydroxy-4-phenyl Butanoic Acid (12b). Mp 148 °C. ^{1}H NMR (360 MHz, DMSO-d_6) δ 1.27 (s, 9H), 2.66−2.68 (m, 2H), 3.92−4.00 (m, 2H), 6.66 (d, J = 9.0 Hz, 1H, N*H*), 7.16−7.26 (m, 5H). ^{13}C NMR (90 MHz, DMSO-d_6) δ 28.1, 34.9, 54.5, 72.6, 77.5, 125.8, 127.9, 129.0, 139.2, 154.9, 173.9.

(2S,3R)-N-(tert-Butoxycarbonyl)-3-amino-2-hydroxy-4-phenyl Butanoic Acid (13b). Mp 126 °C. ^{1}H NMR (360 MHz, DMSO-d_6) δ 1.30 (s, 9H), 2.66−2.71 (m, 1H), 2.78−2.83 (m, 1H), 3.96−4.03 (m, 1H), 5.14 (br s, 1H), 6.37 (d, J = 9.4 Hz, 1H, N*H*), 7.17−7.30 (m, 5H), 12.5 (s, 1H). ^{13}C NMR (90 MHz, DMSO-d_6) δ 27.7, 28.1, 37.5, 54.7, 70.4, 77.8, 126.0, 128.1, 129.1, 138.6, 154.8, 174.0.

(2R,3R)-N-(tert-Butoxycarbonyl)-3-amino-2-hydroxy-4-(p-methyloxyphenyl)-butanoic Acid (12c). ^{1}H NMR (360 MHz, DMSO-d_6) δ 1.28 (s, 9H), 2.60−2.62 (m, 2H), 3.70 (s, 3H), 3.36−3.88 (m, 1H), 3.99−4.0 (m, 1H), 6.53 (d, J = 8.6 Hz, 1H, N*H*), 6.81 (d, J = 8.6 Hz, 2H), 7.08 (d, J = 8.6 Hz, 2H). ^{13}C NMR (90 MHz, DMSO-d_6) δ 28.1, 33.9, 54.7, 54.9, 72.5, 77.5, 107.8, 113.4, 129.9, 130.9, 154.9, 157.5, 174.0.

(2S,3R)-(tert-Butoxycarbonyl)-3-amino-2-hydroxy-4-(p-methyloxyphenyl)-butanoic Acid (13c). Mp 55 °C. ^{1}H NMR (360 MHz, DMSO-d_6) δ 1.33 (s, 9H), 2.632.65 (m, 1H), 2.71−2.73 (m, 1H), 3.72 (s, 3H), 3.84−3.94 (m, 2H), 6.32 (d, J = 9.36 Hz, 1H, N*H*), 6.84 (d, J = 8.6 Hz, 2H), 7.12 (d, J = 8.6 Hz, 2H). ^{13}C NMR (90 MHz, DMSO-d_6) δ 27.8, 28.2, 36.6, 54.9, 55.0, 70.3, 77.8, 113.7, 130.1, 130.5, 154.9, 157.7, 174.1. HRMS calcd for $C_{16}H_{24}NO_6$ (M^+ + H) 326.1598, found 326.1599.

(2R,3R)-N-(tert-Butoxycarbonyl)-3-amino-2-hydroxy-4-(p-benzyloxy phenyl)-butanoic Acid (12d). Mp 129 °C. ^{1}H NMR (360 MHz, DMSO-d_6) δ 1.27 (s, 9H), 2.60−2.61 (m, 2H), 3.85−3.86 (m, 1H), 3.96−3.99 (m, 1H), 5.04 (s, 2H), 6.61 (d, J = 8.6 Hz, 1H, N*H*), 6.88 (d, J = 8.3 Hz, 2H), 7.08 (d, J = 8.3 Hz, 2H), 7.31−7.43 (m, 5H). ^{13}C NMR (90 MHz, DMSO-d_6) δ 28.1, 33.9, 54.7, 69.1, 72.5, 77.5, 114.3, 127.5, 127.7, 128.3, 130.0, 131.2, 137.3, 155.0, 156.6, 174.0.

(2S,3R)-N-(tert-Butoxycarbonyl)-3-amino-2-hydroxy-4-(p-benzyloxyphenyl)-butanoic Acid (13d). Mp 52 °C; $[\alpha]_D^{25}$ = +56.84 (c = 0.19, MeOH). ^{1}H NMR (360 MHz, DMSO-d_6) δ 1.31 (s, 9H), 2.62−2.66 (m, 1H), 2.72−2.74 (m, 1H), 3.86−3.96 (m, 2H), 5.05 (s, 2H), 6.33 (d, J = 9.4 Hz, 1H, N*H*), 6.93 (d, J = 8.6 Hz, 2H), 7.13 (d, J = 8.6 Hz, 2H), 7.31−7.44 (m, 5H). ^{13}C NMR (90 MHz, DMSO-d_6) δ 28.1, 36.6, 54.9, 69.2, 70.3, 77.8, 114.6, 127.6, 127.7, 128.4, 130.2, 130.7, 137.2, 154.9, 156.9, 174.1. HRMS calcd for $C_{22}H_{27}NO_6$ (M^+ − H) = 400.1760, found =400.1755.

(2R,3R)-N-(tert-Butoxycarbonyl)-3-amino-2-hydroxy-4-(2-naphtyl)-butanoic Acid (12e). Yield 77%; mp 154−155 °C. ^{1}H NMR (360 MHz, DMSO-d_6) δ 1.20 (s, 9H), 2.84−2.86 (m, 2H), 4.01−4.04 (m, 2H), 6.72 (d, J = 8.6 Hz, 1H, N*H*), 7.34−7.47 (m, 3H), 7.66 (s, 1H), 7.79−7.86 (m, 3H).

(2S,3R)-N-(tert-Butoxycarbonyl)-3-amino-2-hydroxy-4-(2-naphtyl)-butanoic Acid (13e). Mp 113 °C; $[\alpha]_D^{25}$ = +55.18 (c = 0.54, MeOH). ^{1}H NMR (360 MHz, DMSO-d_6) δ 1.26 (s, 9H), 2.88−2.90 (m, 1H), 2.97−2.99 (m, 1H), 3.93 (s, 1H), 4.11−4.13 (m, 1H), 6.42 (d, J = 9.7 Hz, 1H, N*H*), 7.39−7.48 (m, 3H), 7.71 (s, 1H), 7.82−7.87 (m, 3H). ^{13}C NMR (90 MHz, DMSO-d_6) δ 28.1, 37.7, 54.7, 70.6, 77.8, 125.3, 125.9, 127.3, 127.4, 127.4, 127.6, 127.8, 131.8, 133.1, 136.2, 154.9, 174.0. HRMS calcd for $C_{19}H_{23}NO_5$ (M^+ − H) = 344.1498, found = 344.1497.

(2R,3R)-N-(tert-Butoxycabonyl)-3-amino-2-hydroxy-4-(p-phenylphenyl)-butanoic Acid (12f). ^{1}H NMR (360 MHz, DMSO-d_6) δ 1.27 (s, 9H), 2.73 (br s, 2H), 3.95−4.03 (m, 2H), 6.71 (d, J = 8.8 Hz, 1H, N*H*), 7.26−7.63 (m, 9H). ^{13}C NMR (90 MHz, DMSO-d_6) δ 27.7, 28.1, 34.5, 54.6, 72.6, 77.5, 126.2, 126.4, 127.1, 128.8, 129.6, 137.7, 138.5, 140.1, 155.0, 174.0.

(2S,3R)-N-(tert-Butoxycarbonyl)-3-amino-2-hydroxy-4-(p-phenylphenyl)-butanoic Acid (13f). Mp 162−163 °C. ^{1}H NMR (360 MHz, DMSO-d_6) δ ; 1.31 (s, 9H), 2.73−2.76 (m, 1H), 2.83−2.89

(m, 1H), 3.92−4.04 (m, 2H), 6.39 (d, J = 9.4 Hz, 1H, N*H*), 7.29−7.64 (m, 9H). ^{13}C NMR (90 MHz, DMSO-d_6) δ 27.7, 28.1, 37.1, 54.7, 70.5, 77.8, 126.5, 127.2, 128.9, 129.8, 129.9, 137.9, 138.0, 140.0, 154.9, 174.0. HRMS calcd for $C_{21}H_{25}NO_5$ ($M^+ - H$) = 370.1654, found = 370.1650.

N-(tert-Butoxycarbonyl)-3-amino-4,4-diphenyl-2-hydroxypentanoic Acid (12g). ^{1}H NMR (360 MHz, DMSO-d_6) δ 1.18 (s, 9H), 3.68 (s, 1H), 4.21 (d, J = 11.8 Hz, 1H), 4.79 (t, J = 11.6 Hz, 1H), 6.24 (d, J = 10.04 Hz, 1H, N*H*), 7.08−7.37 (m, 10H). ^{13}C NMR (90 MHz, DMSO-d_6) δ 27.7, 27.9, 53.1, 55.1, 69.6, 77.6, 125.9, 126.5, 127.9, 128.0, 128.4, 128.7, 142.2, 142.5, 154.8, 174.0. HRMS calcd for $C_{21}H_{25}NO_5$ ($M^+ - H$) = 370.1654, found = 370.1655.

N-(tert-Butoxycarbonyl)-3-amino-2-hydroxy-4-propylbutanoic Acid (12h). ^{1}H NMR (360 MHz, DMSO-d_6) δ 0.83 (t, 3H, J = 6.8 Hz), 1.15−1.40 (m, 15H), 3.67−3.69 (m, 1H), 3.92 (d, 1H, J = 4.3 Hz), 6.44 (d, 1H, J = 9 Hz). ^{13}C NMR (90 MHz, DMSO-d_6) δ 13.8, 21.9, 27.7, 28.2, 28.3, 52.6, 72.6, 77.5, 120.7, 155.3, 174.1. ESIMS calcd for $C_{12}H_{23}NO_5$ ($M^+ + H$) = 261.1, found = 284.1 ($M^+ + 23$).

*General Procedure for the Synthesis of Bestatin (**1**) and its P1 Derivatives (**14**−**20**).* Standard solid-phase peptide synthesis was performed on LeuWang resin. Coupling of the α-hydroxy-β-amino acid required HATU for 1 h. Fmoc protecting groups were removed with 20% piperidine/DMF (30 min). To cleave products from resin, a solution of 95%TFA:2.5% TIS:2.5%H_2O was added to the resin. After standing for 2 h, the cleavage mixture was collected and the resin was washed with fresh cleavage solution. The combined fractions were evaporated to dryness, and the product was purified by reverse phase-HPLC. Fractions containing product were pooled and lyophilized. The yields of bestatin (**1**) and its derivatives **14**−**20** ranged from 60% to 70%, respectively.

HRMS calcd for LeuLeuOH **14** $C_{13}H_{27}N_2O_4$ ($M^+ + H$) 275.1965, found 275.1973.

HRMS calcd for Tyr(OMe)LeuOH **15** $C_{17}H_{27}N_2O_5$ ($M^+ + H$) 339.1914, found 339.1913.

HRMS calcd for Tyr(OBzl)LeuOH **16** $C_{23}H_{31}N_2O_5$ ($M^+ + H$) 415.2227, found 415.2221.

ESIMS calcd for NaphLeuOH **17** $C_{20}H_{27}N_2O_4$ ($M^+ + H$) 359.1, found 359.1, 330.2 ($M^+ - 29$).

ESIMS calcd for BipLeuOH **18** $C_{22}H_{30}N_2O_4$ ($M^+ + H$) 385.2, found 385.1, 355.1 ($M^+ - 29$).

ESIMS calcd for DipLeuOH **19** $C_{22}H_{30}N_2O_4$ ($M^+ + H$) 385.2, found 355.1 ($M^+ - 29$).

ESIMS calcd for NleLeuOH **20** $C_{13}H_{26}N_2O_4$ ($M^+ + H$) 275.1965, found 275.1964.

■ ASSOCIATED CONTENT

Ⓢ Supporting Information. ^{1}H and ^{13}C NMR spectra and LCMS profiles of compounds. This material is available free of charge via the Internet at http://pubs.acs.org.

Accession Codes

†PDB ID Codes: The coordinates and structure factors are available from the Protein Data Bank (3Q43 and 3Q44).

■ AUTHOR INFORMATION

Corresponding Author

*Phone: (+)1-215-746-2992, Fax: (+)1-215-746-6697, E-mail: dorong@mail.med.upenn.edu.

■ ACKNOWLEDGMENT

D.C.G. acknowledges support from McCabe Pilot Award, Penn Genome Frontiers Institute, 1R56AI081770-01A2, and the Ritter Foundation. M.B.H. is supported by NIH training grant 5T32AI007532. M.K. is supported by NIH grant AI077638. J.C. W. is an Australian Research Council Federation Fellow and a National Health and Medical Research Council (NHMRC) Principal Research Fellow. We thank the NHMRC and the ARC for funding support. We thank the Australian Synchrotron for beamtime and Tom Caradoc-Davis in particular for technical assistance.

■ ABBREVIATIONS USED

Pf-LAP, *Plasmodium falciparum*-leucine amino peptidase; Tyr(OMe), *p*-methoxy phenyl; Tyr(OBzl), *p*-benzyloxy phenyl; Boc, *tert*-butyloxy carbonyl; DIEA, *N*,*N*-diisopropylethylamine; DMAP, 4-dimethylaminopyridine; HATU, (2-(7-aza-1*H*-benzotriazole-1-yl)-1,1,3,3-tetramethyluronium hexafluorophosphate); DBU, 1,8-diazabicyclo[5.4.0]undec-7-ene; Fmoc, fluorenylmethyloxycarbonyl; TFA, trifluoroacetic acid; TIS, triisopropyl silane; EDAC·HCl, *N*-(3-dimethylaminopropyl)-*N*′-ethylcarbodiimide hydrochloride; TEMPO, 2,2,6,6-tetramethylpiperidine-1-oxyl

■ REFERENCES

(1) Snow, R. W.; Guerra, C. A.; Noor, A. M.; Myint, H. Y.; Hay, S. I. The global distribution of clinical episodes of *Plasmodium falciparum* malaria. *Nature* **2005**, *434*, 214–217.

(2) Francis, S. E.; Sullivan, D. J., Jr.; Goldberg, D. E. Hemoglobin metabolism in the malaria parasite *Plasmodium falciparum*. *Annu. Rev. Microbiol.* **1997**, *51*, 97–123.

(3) Liu, J.; Istvan, E. S.; Gluzman, I. Y.; Gross, J.; Goldberg, D. E. *Plasmodium falciparum* ensures its amino acid supply with multiple acquisition pathways and redundant proteolytic enzyme systems. *Proc. Natl. Acad. Sci. U.S.A.* **2006**, *103*, 8840–8845.

(4) Chen, X.; Chong, C. R.; Shi, L.; Yoshimoto, T.; Sullivan, D. J., Jr.; Liu, J. O. Inhibitors of *Plasmodium falciparum* methionine aminopeptidase 1b possess antimalarial activity. *Proc. Natl. Acad. Sci. U.S.A.* **2006**, *103*, 14548–14553.

(5) Chen, X.; Xie, S.; Bhat, S.; Kumar, N.; Shapiro, T. A.; Liu, J. O. Fumagillin and fumarranol interact with *P. falciparum* methionine aminopeptidase 2 and inhibit malaria parasite growth in vitro and in vivo. *Chem. Biol.* **2009**, *16*, 193–202.

(6) Dalal, S.; Klemba, M. Roles for two aminopeptidases in vacuolar hemoglobin catabolism in *Plasmodium falciparum*. *J. Biol. Chem.* **2007**, *282*, 35978–35987.

(7) Luan, Y.; Xu, W. The structure and main functions of aminopeptidase N. *Curr. Med. Chem.* **2007**, *14*, 639–647.

(8) Sato, Y. Role of aminopeptidase in angiogenesis. *Biol. Pharm. Bull.* **2004**, *27*, 772–776.

(9) Foulon, T.; Cadel, S.; Cohen, P. Aminopeptidase B (EC 3.4.11.6). *Int. J. Biochem. Cell Biol.* **1999**, *31*, 747–750.

(10) Giannousis, P. P.; Bartlett, P. A. Phosphorus amino acid analogues as inhibitors of leucine aminopeptidase. *J. Med. Chem.* **1987**, *30*, 1603–1609.

(11) Chan, W. W.; Dennis, P.; Demmer, W.; Brand, K. Inhibition of leucine aminopeptidase by amino acid hydroxamates. *J. Biol. Chem.* **1982**, *257*, 7955–7957.

(12) Wilkes, S. H.; Prescott, J. M. The slow, tight binding of bestatin and amastatin to aminopeptidases. *J. Biol. Chem.* **1985**, *260*, 13154–13162.

(13) Rich, D. H.; Moon, B. J.; Harbeson, S. Inhibition of aminopeptidases by amastatin and bestatin derivatives. Effect of inhibitor structure on slow-binding processes. *J. Med. Chem.* **1984**, *27*, 417–422.

(14) Suda, H.; Aoyagi, T.; Takeuchi, T.; Umezawa, H. Inhibition of aminopeptidase B and leucine aminopeptidase by bestatin and its stereoisomer. *Arch. Biochem. Biophys.* **1976**, *177*, 196–200.

(15) Burley, S. K.; David, P. R.; Lipscomb, W. N. Leucine aminopeptidase: bestatin inhibition and a model for enzyme-catalyzed peptide hydrolysis. *Proc. Natl. Acad. Sci. U.S.A.* **1991**, *88*, 6916–6920.

(16) Tsuge, H.; Ago, H.; Aoki, M.; Furuno, M.; Noma, M.; Miyano, M.; Minami, M.; Izumi, T.; Shimizu, T. Crystallization and preliminary

X-ray crystallographic studies of recombinant human leukotriene A4 hydrolase complexed with bestatin. *J. Mol. Biol.* **1994**, *238*, 854–856.

(17) Addlagatta, A.; Gay, L.; Matthews, B. W. Structure of aminopeptidase N from *Escherichia coli* suggests a compartmentalized, gated active site. *Proc. Natl. Acad. Sci. U.S.A.* **2006**, *103*, 13339–13344.

(18) Nankya-Kitaka, M. F.; Curley, G. P.; Gavigan, C. S.; Bell, A.; Dalton, J. P. *Plasmodium chabaudi chabaudi* and *P. falciparum*: inhibition of aminopeptidase and parasite growth by bestatin and nitrobestatin. *Parasitol. Res.* **1998**, *84*, 552–558.

(19) Chauvel, E. N.; Llorens-Cortes, C.; Coric, P.; Wilk, S.; Roques, B. P.; Fournie-Zaluski, M. C. Differential inhibition of aminopeptidase A and aminopeptidase N by new beta-amino thiols. *J. Med. Chem.* **1994**, *37*, 2950–2957.

(20) McGowan, S.; Porter, C. J.; Lowther, J.; Stack, C. M.; Golding, S. J.; Skinner-Adams, T. S.; Trenholme, K. R.; Teuscher, F.; Donnelly, S. M.; Grembecka, J.; Mucha, A.; Kafarski, P.; Degori, R.; Buckle, A. M.; Gardiner, D. L.; Whisstock, J. C.; Dalton, J. P. Structural basis for the inhibition of the essential *Plasmodium falciparum* M1 neutral aminopeptidase. *Proc. Natl. Acad. Sci. U.S.A.* **2009**, *106*, 2537–2542.

(21) Harbut, M. B.; Velmourougane, G.; Reiss, G.; Chandramohanadas, R.; Greenbaum, D. C. Development of bestatin-based activity-based probes for metallo-aminopeptidases. *Bioorg. Med. Chem. Lett.* **2008**, *18*, 5932–5936.

(22) Suda, H.; Takita, T.; Aoyagi, T.; Umezawa, H. The chemical synthesis of bestatin. *J. Antibiot.* **1976**, *29*, 600–601.

(23) Lee, B. W.; Lee, J. H.; Jang, K. C.; Kang, J. E.; Kim, J. H.; Park, K.-M.; Park, K. H. Diastereoselective synthesis of *syn*-aminoalcohols via contributing CH−[pi] interaction: simple synthesis of (−)-bestatin. *Tetrahedron Lett.* **2003**, *44*, 5905–5907.

(24) Kobayashi, S.; Isobe, T.; Ohno, M. A stereocontrolled synthesis of (−)-bestatin from an acyclic allylamine by iodocyclocarbamation. *Tetrahedron Lett.* **1984**, *25*, 5079–5082.

(25) Govindaswamy, M.; Motomu, K.; Groger, H.; Shibasaki, M. Anti- and syn-selective cyanosilylation reactions promoted by a sugar-based bifunctional catalyst: stereoselective syntheses of essential building blocks for HIV protease inhibitors and bestatin. *Synlett* **2001**, *5*, 617–620.

(26) Koseki, K.; Matsushita, H. Synthesis of Bestatin, a potent inhibitor of leukotriene A4 hydrolase, by an N3 nucleophile. *Biosci., Biotechnol., Biochem.* **1996**, *60*, 534–536.

(27) Levene, P. A. S., E. T. Acetone derivatives of D-ribose. *J. Biol. Chem.* **1933**, *102*, 187–201.

(28) Bergmeier, S. C.; Stanchina, D. M. Acylnitrene Route to Vicinal Amino Alcohols. Application to the Synthesis of (−)-Bestatin and Analogues. *J. Org. Chem.* **1999**, *64*, 2852–2859.

(29) Lee, J. H.; Jang, K. C.; Jeong, I.-Y.; Yang, M. S.; Lee, S. G.; Park, K. H. Chirospecific synthesis of the (2*S*,3*R*)- and (2*S*,3*S*)-3-amino-2-hydroxy-4-phenylbutanoic acids from sugar: Application to (−)-Bestatin. *Synthesis* **2003**, *6*, 829–836.

(30) Gogoi, N.; Boruwa, J.; Barua, N. C. A total synthesis of (−)-bestatin using Shibasaki's asymmetric Henry reaction. *Tetrahedron Lett.* **2005**, *46*, 7581–7582.

(31) George, S.; Suryavanshi, G. S.; Sudalai, A. A short enantioselective synthesis of (−)-bestatin via l-proline-catalyzed [alpha]-amination of an aldehyde. *Tetrahedron Lett.* **2008**, *49*, 6791–6793.

(32) Rubin, A. E.; Sharpless, K. B. A Highly Efficient Aminohydroxylation Process. *Angew. Chem., Int. Ed. Engl.* **1997**, *36*, 2637–2640.

(33) Donohoe, T. J.; Johnson, P. D.; Pye, R. J. The tethered aminohydroxylation (TA) reaction. *Org. Biomol. Chem.* **2003**, *1*, 2025–2028.

(34) Fraser, D. S.; Park, S. B.; Chong, J. M. Diastereoselective reduction of alpha-aminoketones: synthesis of *anti*- and *syn*-beta-aminoalcohols. *Can. J. Chem.* **2004**, *82*, 87–101.

(35) Anand, N.; Kapoor, M.; Koul, S.; Taneja, S. C.; Sharma, R. L.; Qazi, G. N. Chemoenzymatic approach to optically active phenylglycidates: resolution of bromo- and iodohydrins. *Tetrahedron: Asymmetry* **2004**, *15*, 3131–3138.

(36) Feske, B. D.; Stewart, J. D. Chemoenzymatic formal total synthesis of (−)-bestatin. *Tetrahedron: Asymmetry* **2005**, *16*, 3124–3127.

(37) Semple, J. E.; Owens, T. D.; Nguyen, K.; Levy, O. E. New Synthetic Technology for Efficient Construction of alpha-Hydroxy-beta-amino Amides via the Passerini Reaction. *Org. Lett.* **2000**, *2*, 2769–2772.

(38) Herranz, R.; Castro-Pichel, J.; Vinuesa, S.; Garcia-Lopez, M. T. An improved one-pot method for the stereoselective synthesis of the (2*S*,3*R*)-3-amino-2-hydroxy acids: key intermediates for bestatin and amastatin. *J. Org. Chem.* **1990**, *55*, 2232–2234.

(39) So, R. C.; Ndonye, R.; Izmirian, D. P.; Richardson, S. K.; Guerrera, R. L.; Howell, A. R. Straightforward Synthesis of Sphinganines via a Serine-Derived Weinreb Amide. *J. Org. Chem.* **2004**, *69*, 3233–3235.

(40) de Koning, M. C.; Petersen, L.; Weterings, J. J.; Overhand, M.; van der Marel, G. A.; Filippov, D. V. Synthesis of thiol-modified peptide nucleic acids designed for post-assembly conjugation reactions. *Tetrahedron* **2006**, *62*, 3248–3258.

(41) McKillop, A. T.; Watson, R. J.; Lewis, N. An improved procedure for the preparation of the garner aldehyde and its use for the synthesis of N-protected 1-halo-2-(*R*)-amino-3-butenes. *Synthesis* **1994**, 31–33.

(42) Cong, X.; Liao, Q.-J.; Yao, Z.-J. RCM Approaches toward the Diastereoselective Synthesis of Vicinal *trans*-Diaminocyclitols from l-Serine. *J. Org. Chem.* **2004**, *69*, 5314–5321.

(43) Wovkulich, P. M.; Shankaran, K.; Kiegiel, J.; Uskokovic, M. R. Total synthesis of 1233A. *J. Org. Chem.* **1993**, *58*, 832–839.

(44) Zhao, M.; Li, J.; Mano, E.; Song, Z.; Tschaen, D. M.; Grabowski, E. J. J.; Reider, P. J. Oxidation of Primary Alcohols to Carboxylic Acids with Sodium Chlorite Catalyzed by TEMPO and Bleach. *J. Org. Chem.* **1999**, *64*, 2564–2566.

(45) Nishizawa, R.; Saino, T.; Takita, T.; Suda, H.; Aoyagi, T. Synthesis and structure−activity relationships of bestatin analogues, inhibitors of aminopeptidase B. *J. Med. Chem.* **1977**, *20*, 510–515.

(46) Stockel-Maschek, A.; Stiebitz, B.; Koelsch, R.; Neubert, K. Novel 3-amino-2-hydroxy acids containing protease inhibitors. Part 1: Synthesis and kinetic characterization as aminopeptidase P inhibitors. *Bioorg. Med. Chem.* **2005**, *13*, 4806–4820.

(47) Skinner-Adams, T. S.; Stack, C. M.; Trenholme, K. R.; Brown, C. L.; Grembecka, J.; Lowther, J.; Mucha, A.; Drag, M.; Kafarski, P.; McGowan, S.; Whisstock, J. C.; Gardiner, D. L.; Dalton, J. P. *Plasmodium falciparum* neutral aminopeptidases: new targets for antimalarials. *Trends Biochem. Sci.* **2010**, *35*, 53–61.

(48) Potterton, L.; McNicholas, S.; Krissinel, E.; Gruber, J.; Cowtan, K.; Emsley, P.; Murshudov, G. N.; Cohen, S.; Perrakis, A.; Noble, M. Developments in the CCP4 molecular-graphics project. *Acta Crystallogr., Sect. D: Biol. Crystallogr.* **2004**, *60*, 2288–2294.

(49) Dixon, M. The determination of enzyme inhibitor constants. *Biochem. J.* **1953**, *55*, 170–171.

(50) Cornish-Bowden, A. A simple graphical method for determining the inhibition constants of mixed, uncompetitive and noncompetitive inhibitors. *Biochem. J.* **1974**, *137*, 143–144.

(51) Trager, W.; Jensen, J. B. Human malaria parasites in continuous culture. *Science* **1976**, *193*, 673–675.

(52) Leslie, A. G. W. Recent changes to the MOSFLM package for processing film and image plate data. *Joint CCP4 + ESF-EAMCB Newsletter on Protein Crystallography* **1992**, *26*, 27−33.

(53) Evans, P. Scaling and assessment of data quality. *Acta Crystallogr., Sect. D: Biol. Crystallogr.* **2006**, *62*, 72–82.

(54) The CCP4 suite: programs for protein crystallography. *Acta Crystallogr., Sect. D: Biol. Crystallogr.* **1994**, *50*, 760−763.

(55) Brunger, A. T. Assessment of phase accuracy by cross validation: the free R value. Methods and applications. *Acta Crystallogr., Sect. D: Biol. Crystallogr.* **1993**, *49*, 24–36.

(56) Potterton, E.; Briggs, P.; Turkenburg, M.; Dodson, E. A graphical user interface to the CCP4 program suite. *Acta Crystallogr., Sect. D: Biol. Crystallogr.* **2003**, *59*, 1131–1137.

(57) Konagurthu, A. S.; Whisstock, J. C.; Stuckey, P. J.; Lesk, A. M. MUSTANG: a multiple structural alignment algorithm. *Proteins* **2006**, *64*, 559–574.

(58) DeLano, W. *The PyMOL Molecular Graphics System*; Scientific D DeLano Scientific: San Carlos, CA USA, 2002.

(59) Androulakis, S.; Schmidberger, J.; Bate, M. A.; DeGori, R.; Beitz, A.; Keong, C.; Cameron, B.; McGowan, S.; Porter, C. J.; Harrison, A.; Hunter, J.; Martin, J. L.; Kobe, B.; Dobson, R. C.; Parker, M. W.; Whisstock, J. C.; Gray, J.; Treloar, A.; Groenewegen, D.; Dickson, N.; Buckle, A. M. Federated repositories of X-ray diffraction images. *Acta Crystallogr., Sect. D: Biol. Crystallogr.* **2008**, *64*, 810–814.